

# Electric Polarizability of DNA in Aqueous Salt Solution

Hitoshi Washizu\*

Toyota Central R&D Labs., Inc., Nagakute, Aichi 480-1192, Japan

Kazuo Kikuchi†

Hino 475-4, Hino-shi, Tokyo 191-0012, Japan

Received: August 2, 2005; In Final Form: December 15, 2005

Monte Carlo simulations are performed to determine the anisotropy of the electric polarizability of a model DNA fragment in aqueous salt solution. By taking into consideration the participation of coions in the electroneutrality condition, at every simulation step, we obtain a list of counterions constituting the net charge arranged in increasing order of their distance from the DNA and calculate the contribution to the dipole moment from the first  $n$  counterions in the list. We define a partial polarizability tensor due to these  $n$  counterions to understand the origin of the polarizability in close relation to the solution structure. The ionic distributions are described by the counterion condensation theory. Characteristic features of the electric properties of polyelectrolytes are reproduced. The anisotropy of the electric polarizability  $\Delta\alpha$  of DNA decreases with the addition of salt, yielding values comparable to experiment. The effect of electrophoretic motion of the polyion is examined by estimating its upper limit.

## 1. Introduction

According to the fluctuation–dissipation theorem,<sup>1</sup> electric polarizability of polyelectrolytes is related to the time-correlation function of the dipole moment spontaneously created in the ion atmosphere around a polyion in the absence of an applied electric field.<sup>2–6</sup> Let  $\mu_s(t)$  be the  $s$ th component of the dipole moment at time  $t$ , then the frequency dependence of the  $r$ st component of the polarizability tensor is given by

$$\alpha_{rs}(\omega) = \frac{1}{k_B T} [\langle \mu_r(0) \mu_s(0) \rangle - i\omega \int_0^\infty \langle \mu_r(0) \mu_s(t) \rangle e^{-i\omega t} dt] \quad (1)$$

where  $\omega$  is the angular frequency,  $k_B$  the Boltzmann constant, and  $T$  the absolute temperature.

The Monte Carlo (MC) Brownian dynamics method<sup>7–11</sup> enables us to calculate concentrations of small ions and the electrical potential as functions of space and time with hydrodynamic interactions between ionic species taken into account. Recently, we started to determine anisotropy of the static electric polarizability  $\Delta\alpha$  of model DNA fragments in aqueous solution by MC simulation<sup>12–20</sup> and reproduced characteristics of the electric properties of polyelectrolytes in both salt-free<sup>19,20</sup> and salt solutions.<sup>17</sup>

The system has prolate ellipsoidal symmetry with the foci located at both ends of the DNA polyion cylinder.<sup>21</sup> In salt-free solutions,<sup>19,20</sup> at every simulation step, we numerically sort counterions in increasing order of the sum of their distances from both ends of the polyion. Two kinds of counterions are distinguished from their spatial distributions and identified in the framework of the counterion condensation theory<sup>3,22,23</sup> as condensed counterions and diffuse ion atmospheres. We define

a partial polarizability tensor by calculating fluctuations of the contribution to the dipole moment from the first  $n$  counterions in the sorting list. Its introduction facilitates understanding the origin of the polarizability in close relation to the solution structure. In salt-free solutions, the anisotropy of the electric polarizability  $\Delta\alpha$  of model DNA fragments increases on dilution of the polymer concentration and is proportional to the second or higher power of the DNA molecular weight consistent with experiment.

In our preliminary report on salt solutions,<sup>17</sup> by taking into consideration the involvement of coions in the electroneutrality condition, at every simulation step, we obtain a list of counterions constituting the net charge that compensates the polyion charge.  $\Delta\alpha$  decreases on addition of salt, yielding values comparable to experiment.

In this paper, we seek the origin of the induced dipole moment of a polyelectrolyte in salt solution, more closely going into structural details. The ionic structure is described by the theory of Ramanathan and Woodbury.<sup>24</sup> Because of the composite nature of the ion atmosphere, i.e., the ion atmosphere is an overlap of a layer of condensed counterions and a charge distribution obtained from a solution to the Poisson–Boltzmann (PB) equation, evaluated as if the linear charge density parameter of charged chains  $\xi = 1$ , partial polarizabilities do not reveal the presence of a condensed counterion layer clearly. Complementary data are also available elsewhere.<sup>25</sup>

Grycuk et al.<sup>26</sup> analyzed the polarization of rodlike polyelectrolytes by Brownian dynamics simulations and calculated induced dipole moments as a function of the external electric field strength, and Antosiewicz and Porschke<sup>27</sup> extended the calculation by including hydrodynamic interactions between component ions. Although their approach provided dynamics of the process,<sup>10</sup> dipole moments calculated showed complex dependence on the various simulation parameters, i.e., electric field strength, polymer concentration, and salt concentration, and clear separation of their influences is very difficult.

\* Corresponding author. E-mail: h@washizu.org. Telephone: +81-561-63-6243. Fax: +81-561-63-6482.

† E-mail: kakikuke@khaki.plala.or.jp. Telephone and Fax: +81-42-586-9827.

**TABLE 1: Salt Concentrations**

salt concentration <sup>a</sup> /mM $c_s$	number of counterions in MC cell	number of coions in MC cell	Debye length <sup>b</sup> /nm $\kappa^{-1}$
0.0	128	0	
0.60	256	128	12.41
1.2	384	256	8.77
2.4	640	512	6.21
4.8	1152	1024	4.38

<sup>a</sup> Calculated by dividing numbers of coions in the MC cell by its volume and used as approximate bulk salt concentrations. <sup>b</sup> Calculated from approximate bulk salt concentrations  $c_s$ .

Furthermore, the  $(\mu_{||} - \mu_{\perp})$  values simulated for the polymer with 40 residues are close to zero level where  $\mu_{||}$  and  $\mu_{\perp}$  are dipoles induced parallel and perpendicular to the external field.

## 2. Model

A 64 base-pair fragment of double-stranded DNA is modeled as an impenetrable cylinder of radius 1.04 nm. The 128 negative phosphate charges are placed along two right-handed helices embedded in the surface of the cylinder. For canonical *B*-DNA, positions of phosphate charges on one strand are expressed in cylindrical polar coordinates as<sup>28</sup>

$$\begin{aligned} r_i &= 0.89 \\ z_i &= 0.208 + 0.34i \\ \theta_i &= 95.2 + 36i, \quad i = 0, \dots, 31 \end{aligned} \quad (2)$$

where the radial and axial distances from and along the helix axis  $r_i$  and  $z_i$ , respectively, are given in nanometers and the angular coordinate  $\theta_i$  in degrees. To generate coordinates of the phosphate charges on the other strand,  $z_i$  and  $\theta_i$  ( $i = 1, \dots, 32$ ) are negated. Equation 2 shows that the distance between two neighboring phosphate charges on each helix is 0.34 nm along the cylinder axis and that they are situated at a depth of  $1.04 - 0.89 = 0.15$  nm from the surface of the DNA cylinder. The DNA cylinder is extended 0.15 nm beyond the terminal phosphate charges at both ends so that its length is  $L = 21.84$  nm. The hydrated univalent counter- and coions are modeled as hard spheres of radius 0.15 nm. Hence, all the distances of closest approach of small ions to the DNA phosphate charges and to each other are set to 0.30 nm. The solvent is treated as a dielectric continuum with the relative permittivity of pure water  $\epsilon_r = 78.3$  at  $T = 298$  K, and dielectric discontinuity between the solvent and the DNA cylinder is neglected.

The MC cell is basically a sphere of radius 2.0 times as long as the DNA cylinder in which the DNA fragment is placed along the  $z$ -axis with its center in common with that of the MC cell, or the origin of the coordinate axes. The DNA concentration  $c_p$  is calculated by assuming that 128 nucleotide residues occupy an effective volume the size of the simulation cell. Salt concentrations  $c_s$  are calculated by dividing numbers of coions in the simulation cell by its volume and used approximately as bulk salt concentrations. They are tabulated in Table 1, along with the Debye lengths  $\kappa^{-1}$  calculated therefrom. Occasionally,  $c_p$  dependence is studied by changing both the radius of the MC cell and the number of coions added.

## 3. Simulation

The conventional Metropolis MC procedure is used to generate a canonical ensemble. The energy of configurations is calculated as a sum of interactions of each small mobile ion in the MC cell with all the other small ions and DNA charges in

the cell. A value of 0.2 nm is used as the maximum ion displacement  $\Omega^{-1}$  allowed for an MC move along each coordinate direction. The new configuration generated by a random move of a single ion is accepted or rejected according to the probability  $\min\{1, \exp(-\Delta U/k_B T)\}$ , where  $\Delta U$  is the change in configurational energy that would result from the move. When a mobile ion escapes from the cell during a move in the Metropolis sampling process, another ion of the same kind is put to the symmetrical position about the center of the MC sphere. Although the Metropolis time scale  $\Delta t$  is fixed by the relation

$$6D\Delta t \Omega^2 = 1 \quad (3)$$

where  $D$  is the diffusion coefficient for the small ion species in water at infinite dilution,<sup>7,8,10,20</sup> we need not relate the Metropolis and physical time scales in this paper as far as we calculate only time averages.

The system has prolate ellipsoidal symmetry with the foci located at both ends of the DNA polyion cylinder.<sup>21</sup> In salt solutions, the role of coions in the ion atmosphere must be taken into account. We consider that the polyion phosphate charge is compensated by the same amount of the net charge as defined below. First, we sort small ions in increasing order of the sum of their distances from both ends of the polyion (more precisely, from the projections of the terminal charges at both ends of the polyion onto the DNA cylinder axis). Then, if we find a coion in the list, we search a nearest consecutive counterion in the list and delete both entries. We continue this process from the beginning of the list until the first 128 consecutive entries are all occupied by counterions that constitute the net charge.

At each simulation step, we calculate the contribution to the dipole moment from the first  $n$  counterions in the list, constituting the net charge  $(\mu_x(n), \mu_y(n), \mu_z(n))$  as follows,

$$\begin{aligned} \mu_x(n) &= \sum_{i=1}^n ex_i \\ \mu_y(n) &= \sum_{i=1}^n ey_i \\ \mu_z(n) &= \sum_{i=1}^n ez_i \end{aligned} \quad (4)$$

where  $e$  is the elementary charge and  $x_i, y_i, z_i$  are the coordinates of the  $i$ th counterion in the list. We then define a partial polarizability tensor due to these  $n$  net charges with its principal components  $\alpha_{xx}(n), \alpha_{yy}(n), \alpha_{zz}(n)$  given by

$$\begin{aligned} \alpha_{xx}(n) &= \langle \mu_x(n)^2 \rangle - \langle \mu_x(n) \rangle^2 / k_B T \\ \alpha_{yy}(n) &= \langle \mu_y(n)^2 \rangle - \langle \mu_y(n) \rangle^2 / k_B T \\ \alpha_{zz}(n) &= \langle \mu_z(n)^2 \rangle - \langle \mu_z(n) \rangle^2 / k_B T \end{aligned} \quad (5)$$

where  $\langle \rangle$  denotes the canonical ensemble or time average. We define longitudinal and transverse components of the partial polarizability  $\alpha_L(n)$  and  $\alpha_T(n)$  and partial anisotropy of polarizability  $\Delta\alpha(n)$  by the following equations:

$$\alpha_L(n) = \alpha_{zz}(n) \quad (6)$$

$$\alpha_T(n) = (\alpha_{xx}(n) + \alpha_{yy}(n))/2 \quad (7)$$

$$\Delta\alpha(n) = \alpha_L(n) - \alpha_T(n) \quad (8)$$

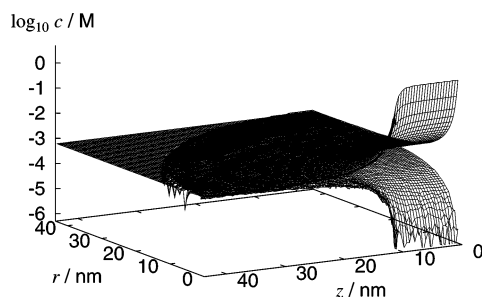


**Figure 1.** Three-dimensional representation of counter- (upper surface) and co- (lower surface) ion concentrations around a 64 base-pair DNA fragment at a polymer concentration  $c_p = 0.60$  mM nucleotide residue and salt concentration  $c_s = 0.60$  mM.

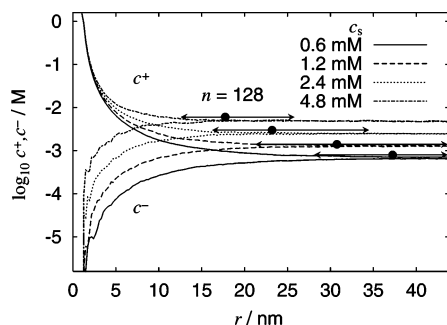


**Figure 2.** Counterion concentration  $c^+$  and coion concentration  $c^-$  profiles for a 64 base-pair DNA at various salt concentrations  $c_s$  as functions of the radial coordinate  $r$  measured from the axis of the DNA cylinder at its center. Bullets represent radial positions where a ridge of high  $P$  (the probability distribution function of finding the outermost net charge) values around the polyion is attained, and arrows represent regions of  $r$  where  $P(r, z = 0)$  is within 90% of the radial maxima.

The anisotropy of the electric polarizability  $\Delta\alpha$  to be determined is expressed as  $\Delta\alpha(128)$ .

#### 4. Results and Discussion

**4.1. Ionic Structure.** Figure 1 shows a global view of counterion concentration  $c^+$  and coion concentration  $c^-$  distributions plotted in logarithmic scale for the lowest salt concentration studied. It is obtained by averaging over  $1.98 \times 10^8$  configurations. The very high counterion concentration ( $\sim 2$  M) and very low coion concentration ( $\sim 10^{-6}$  M) on the surface of the polyion rapidly decreases and increases, respectively, in both radial and longitudinal directions tending to their bulk values.

Figure 2 shows more closely counterion concentration  $c^+$  and coion concentration  $c^-$  profiles as functions of the radial coordinate  $r$  measured from the axis of the DNA cylinder at its center. The ion atmosphere around the polyion is given by the difference of the two curves  $c^+$  and  $c^-$ . Numerical determination of the net charge gives us a boundary between the ion atmosphere and the bulk salt solution, whereas analytical theories do not yield a clear boundary between them. Without truncation or discretization, they merge continuously at infinity.

Let  $P(r, z)$  be the probability distribution function of finding the outermost net charge (the 128th counterion in the sorting list) in the ion atmosphere. In Figure 2, we represent radial positions by bullets where a ridge of high  $P$  values around the polyion is attained and by arrows regions of  $r$  where  $P(r, z = 0)$  is within 90% of the radial maxima. It is seen that the numerical determination of the net charge yields an appropriate boundary between an ion atmosphere and the bulk salt solution.

Figure 3 shows three-dimensional view of the reduced electrostatic potential  $e\psi/k_B T$  around the polyion at a polymer concentration  $c_p = 0.60$  mM nucleotide residue and a salt

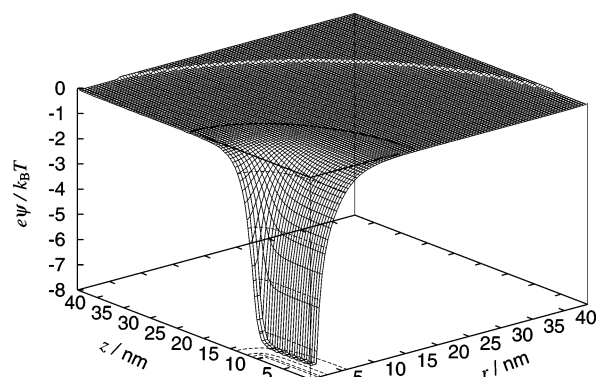


**Figure 3.** Three-dimensional view of the reduced electrostatic potential  $e\psi/k_B T$  around a 64 base-pair DNA at a polymer concentration  $c_p = 0.60$  mM nucleotide residue and a salt concentration  $c_s = 2.4$  mM.

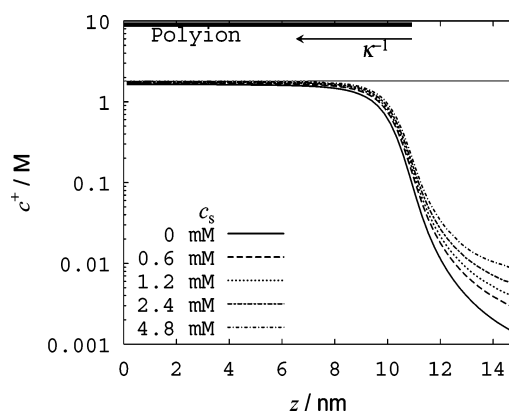


**Figure 4.** Counterion concentration  $c^+$  profiles for a 64 base-pair DNA at various salt concentrations  $c_s$  as functions of the  $z$  coordinate along the surface of the cylinder. Half the length of the polyion  $L/2 = 10.92$  nm and the Debye length  $\kappa^{-1} = 4.38$  nm at the highest salt concentration studied are drawn at the top of the figure.

concentration  $c_s = 2.4$  mM. In the figure, the numerically determined boundary between the ion atmosphere and the bulk salt solution is drawn as well as the MC cell boundary. One notices ellipsoidal symmetry of the electrostatic potential around the oligomer projected on the  $r$ - $z$  plane.

We describe the solution structure in the framework of the counterion condensation theory<sup>3,22,23</sup> extended to finite-length polymers.<sup>24,29</sup> Ramanathan and Woodbury<sup>24</sup> showed that, if the length of the oligomer  $L$  is comparable to  $\kappa^{-1}$  or larger as in the present case, the fractional extent of condensation on the central portion of the polyion is the same as for infinitely long polymers. On the other hand, end effects on condensation were analyzed by Odijk.<sup>30</sup> He showed that the nonuniformity of the number of condensed counterions is limited to within  $\kappa^{-1}$  from the ends of an oligomer. Figure 4 shows counterion concentration  $c^+$  profiles at one end of the polyion. It is seen that end effects are small at the highest salt concentration studied where  $L$  is much larger than  $\kappa^{-1}$ .

Figure 5 shows sum of numbers of counterions  $n^+$  and coions  $n^-$  used to determine the  $n$ th net charge in the sorting list normalized by the total number of DNA phosphate charges  $N = 128$ . Dotted line is the corresponding curve for salt-free solution for which  $n = n^+$ . The figure shows in a discretized manner compared to Figures 1 and 2 that coions are strongly repelled and cannot penetrate into the vicinity of the polyion as far as the latter is neutralized by approximately 98 counterions corresponding to the Manning fraction  $F_M = 0.76$  for DNA in water at 297 K. Participation of a rapidly growing number of coions in the subsequent neutralization process indicates the

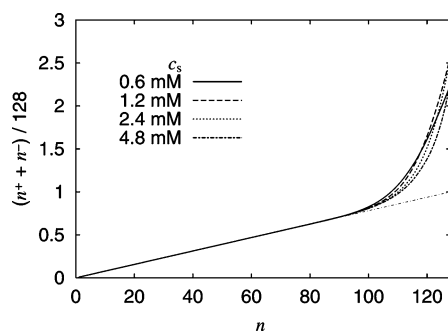


**Figure 5.** Sum of numbers of counterions  $n^+$  and coions  $n^-$  used in the determination of the  $n$ th net charge in the sorting list normalized by the total number of DNA phosphate charges  $N = 128$ . Dotted line is the corresponding curve for salt-free solution for which  $n = n^+$ .

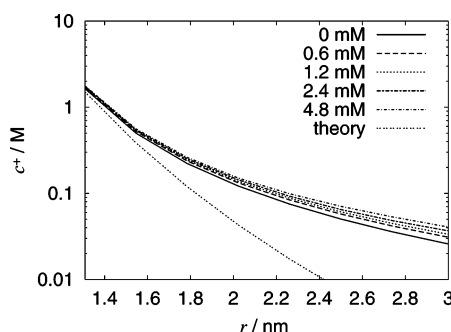


**Figure 6.** Counterion concentration  $c^+$  profiles near the surface of a 64 base-pair DNA as functions of the radial coordinate  $r$  measured from the axis of the DNA cylinder at its center at a polymer concentration  $c_p = 0.60$  mM nucleotide residue. Ramanathan–Woodbury theoretical curve for the distribution of condensed counterions is also drawn.

presence of surrounding diffuse ion atmospheres. These characteristics are as if the ionic structure were described in terms of the Oosawa–Manning two-phase model.<sup>3,22,23</sup>

Figure 5 also shows that ion atmospheres are composed of  $\sim 2.5 N$  ions with the crossings of curves found in the diffuse ion atmosphere region, suggesting occurrence of some structural change in the outer part of the ion atmosphere with the addition of salt.

According to Ramanathan and Woodbury,<sup>24</sup> however, our net charge is an overlap of a layer of condensed counterions and a charge distribution obtained from a solution to the PB equation that is evaluated as if  $\xi = 1$ . Figure 6 shows counterion concentration  $c^+$  profiles near the surface of a 64 base-pair DNA as functions of the radial coordinate  $r$  measured from the axis of the DNA cylinder at its center along with Ramanathan–Woodbury theoretical distribution of condensed counterions that is independent of salt concentration. Subtraction of the  $c^+$  curves and the Ramanathan–Woodbury distribution would yield counterion distributions given by the PB equation with  $\xi = 1$ . It is seen that they have finite values on the surface of the DNA cylinder. As pointed out by Manning,<sup>31</sup> it may be of interest to compare these distributions with the overall distribution determined for a polymer having a unit  $\xi$  value.

Because of the composite nature of the ion atmosphere in salt solution, i.e., an overall charge distribution is produced by an overlap of individually continuous components, a layer of condensed counterions and small ion distributions calculated from a solution to the PB equation, it is not as easy to disclose the presence of a condensed counterion layer from simulation as in salt-free solution where corresponding two components are nonoverlapping discontinuous distributions “glued” together at the point of discontinuity.<sup>31</sup>

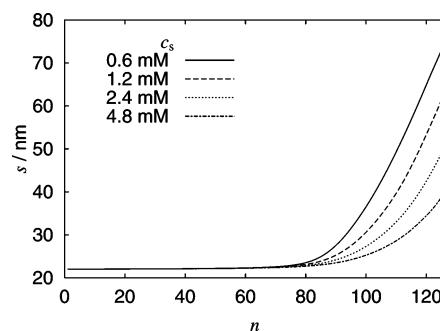


**Figure 7.** Distances  $s$  from the DNA polyion of 128 counterions constituting the net charge or sums of their distances from both ends of the polyion sorted in increasing order  $n$  at every simulation step and averaged over a number of uncorrelated counterion configurations.

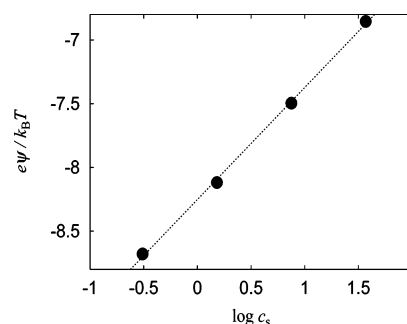


**Figure 8.** Variation of reduced electrostatic potential  $e\psi/k_B T$  on the central surface of a 64 base-pair DNA cylinder with salt concentration  $c_s$  at a polymer concentration  $c_p = 0.60$  mM nucleotide residue.

Figure 7 shows distances from the DNA polyion  $s$  of 128 counterions, constituting the net charge or sums of their distances from both ends of the polyion sorted in increasing order  $n$  at every simulation step and averaged over a number of uncorrelated counterion configurations. Although it is seen that counterions apparently comparable to the Manning fraction are located in the immediate vicinity of the polyion, it is hard to find unique points on the curves that single out condensed counterions as in a salt-free solution.<sup>20</sup> Even the composition of counterions in the immediate vicinity of the polyion cannot be accounted for solely by condensed counterions. As Figure 6 shows, Ramanathan–Woodbury distribution and supposed counterion distributions from the PB equation take approximately the same value 0.1 M at  $r \approx 1.8$  nm. This  $r$  value corresponds to  $s \approx 22.2$  nm or  $n = 52$ –55.

Partial polarizabilities  $\alpha_L(n)$  and  $\alpha_T(n)$  when plotted against  $n$  will show similar behavior because a condensed layer and a charge distribution obtained from a PB solution must exhibit the same electric properties in the region where they are overlapped. Although study of a polymer with  $\xi = 1$  may give us some insight, insofar as we cannot clearly resolve the two components, we must be content with the partial polarizabilities themselves. Because they are obtained by sorting electrostatic potentials felt by small ions, they themselves can provide us with enough information about spatial distributions of counterions to seek the origin of the induced dipole moment of polyelectrolytes.

Figure 8 shows the reduced electrostatic potential  $e\psi/k_B T$  on the central surface of the DNA cylinder as a function of the logarithm of salt concentration  $c_s$ . In accordance with the theory,<sup>24</sup> a linear dependence is obtained.

**4.2. Electric Polarizability.** Figure 9 plots against the number  $n$  of contributing counterions that constitute the net charge longitudinal and transverse partial electric polarizability pairs



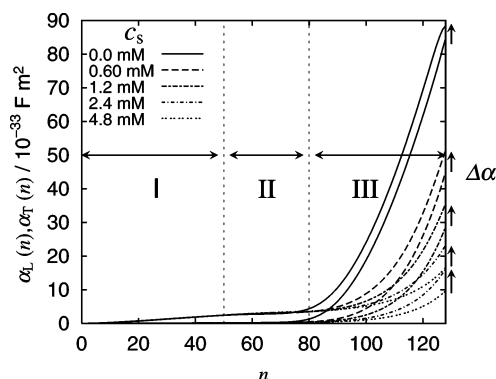


**Figure 9.** Longitudinal and transverse partial electric polarizability pairs  $\alpha_L(n)$  and  $\alpha_T(n)$  for a 64 base-pair DNA fragment at a polymer concentration  $c_p = 0.60$  mM nucleotide residue and various salt concentrations  $c_s$ . For each pair of curves, the upper one is  $\alpha_L(n)$  and the lower one is  $\alpha_T(n)$ . Anisotropy  $\Delta\alpha$  is given by the difference of  $\alpha_L(128)$  and  $\alpha_T(128)$ , as indicated by the arrows on the right-hand side.

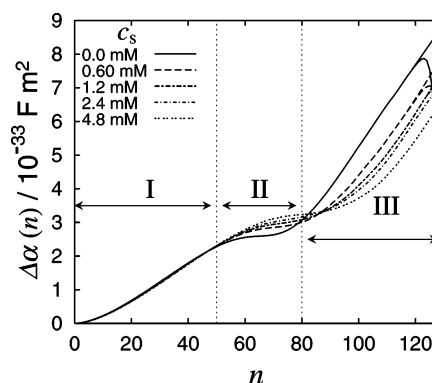
$\alpha_L(n)$  and  $\alpha_T(n)$  determined at various salt concentrations  $c_s$ . For each pair of curves, the upper one is  $\alpha_L(n)$  and the lower one  $\alpha_T(n)$ . We can observe three regions showing different dependence upon  $n$ : region I ( $1 \leq n \leq 50$ ), region II ( $50 \leq n \leq 70$ – $100$ ), and region III ( $70$ – $100 \leq n \leq 128$ ). In region I,  $\alpha(n)$  curves rise from 0 until the DNA phosphate charge is neutralized by about 50 counterions. In region II, they reach plateau values, and in region III, they grow rapidly again.

When  $n$  belongs to region I and II,  $\alpha_T(n)$  remains very small because ions exist in a thin layer over the DNA surface. On the other hand,  $\alpha_L(n)$  increases linearly with  $n$  in region I, as buildup of the  $z$  component of the partial dipole moment  $\mu_z(n)$  is regarded as a random walk starting from the origin of the coordinates. When  $n$  increases over 50, fluctuations of  $\mu_z(n)$  no longer increase with  $n$  as far as  $n$  remains in region II because ions distribute uniformly along the DNA. When  $n$  exits from region II, ion distributions become diffuse, resulting in a rapid increase of both  $\alpha_L(n)$  and  $\alpha_T(n)$ . Anisotropy  $\Delta\alpha$  is given by the difference of two large quantities  $\alpha_L(128)$  and  $\alpha_T(128)$ , as indicated by arrows on the right-hand side of Figure 9.

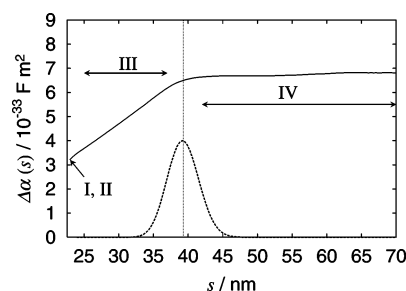
It is seen that the curve for salt-free solution ( $c_s = 0.0$  mM) shows a curvature between region II and III great enough to find a unique point disclosing the presence of a condensed counterion layer.<sup>20</sup> It is also found that the difference in the phosphate charge arrangement of DNA models, linear or double-helical array of charges along the cylinder, has little effect on the calculated polarizability compared to that of our previous results.<sup>20</sup>

Figure 10 plots against the number  $n$  of contributing net charges partial electric polarizability anisotropy  $\Delta\alpha(n)$  determined at various salt concentrations  $c_s$ . We can observe exactly the same regions as in Figure 9. In region I,  $\Delta\alpha(n)$  curves rise from 0 until the DNA phosphate charge is neutralized by about 50 counterions. In region II, they reach plateau values, and in region III, they grow rapidly again.  $\Delta\alpha(n)$  in region III is given as a difference of two large quantities. The ionic structure in this region is still anisotropic and the longitudinal component exhibits larger dependence on  $n$  than the radial, resulting in a sharp increase of the anisotropy. This is because the former originates from displacements of counterions along electrostatic equipotential surfaces and the latter perpendicular.

$\Delta\alpha(n)$  curves show no salt dependence in region I, consistent with the fact that coions are strongly repelled and rarely approach the immediate vicinity of the polyion even at the highest salt concentration studied. On the other hand, in region



**Figure 10.** Partial anisotropy of polarizability  $\Delta\alpha(n)$  for a 64 base-pair DNA fragment as functions of number of contributing counterions (net charges)  $n$  at a polymer concentration  $c_p = 0.60$  mM nucleotide residue and various salt concentrations  $c_s$ .



**Figure 11.** Partial anisotropy of polarizability  $\Delta\alpha(s)$  as a function of distance  $s$  of ions from the polyion for a 64 base-pair DNA at a polymer concentration  $c_p = 0.60$  mM nucleotide residue and a salt concentration  $c_s = 4.8$  mM.

II, the presence of coions affects the curves in such a way that  $\Delta\alpha(n)$  increases with the addition of salt. Manning<sup>32</sup> has already explained this effect in his two-phase model of polarizability, as reflecting the decreased resistance to distortion of the condensation layer. In region III, large contribution from diffuse ion atmospheres as well as reversal of the salt concentration dependence of the  $\Delta\alpha(n)$  curves is observed. Sharp drops of curves seen in the outer part of this region can be regarded as being due to the boundary conditions of our simulation cell. Linear portions of the curves are extrapolated to obtain values of  $\Delta\alpha(128)$  or  $\Delta\alpha$ .

Figure 11 shows contribution to the partial anisotropy of the polarizability  $\Delta\alpha(s)$  from all the small ions, counterions, and coions, within distance  $s$  from the polyion plotted in a wider region including region IV or the bulk salt solution. Partial polarizabilities and anisotropy as functions of  $s$  are defined in a similar manner as  $\alpha_L(n)$ ,  $\alpha_T(n)$ , and  $\Delta\alpha(n)$ . A vertical broken line is drawn to indicate the boundary between the ion atmosphere and the bulk salt solution. The bell-shaped curve is the probability distribution function of finding a 128th counterion constituting the net charge at distance  $s$ . In region IV, polarizability components  $\alpha_L$  and  $\alpha_T$  themselves increase but at the same rate,<sup>25</sup> i.e., electric properties are isotropic in this region, resulting in a constant anisotropy  $\Delta\alpha$ .

We have also studied polymer concentration  $c_p$  dependence of the partial anisotropy of the electric polarizability  $\Delta\alpha(n)$  at a salt concentration  $c_s = 4.8$  mM. In calculating  $c_p$  dependence, both the radius of the MC cell and the number of coions are increased. As the system becomes larger, a modified version of the PPPC (particle–particle and particle–cell) method developed by Saito<sup>33</sup> is applied. An MC cell is divided into a number of cubic cells. At every 10 simulation steps, the total charge  $Q_J$  and the total dipole moment  $\mu_J$  of the  $J$ th cubic cell

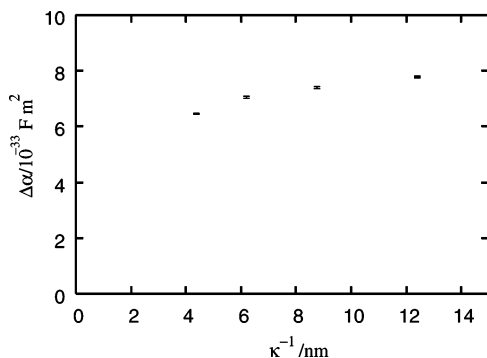


**Figure 12.** Salt concentration  $c_s$  dependence of the anisotropy of electric polarizability  $\Delta\alpha$  for a 64 base-pair DNA at a polymer concentration  $c_p = 0.60$  mM nucleotide residue plotted against the Debye length  $\kappa^{-1}$ .

are calculated and located at its center. The  $i$ th ion feels forces from neighboring charges directly and from cubic cells at large distances collectively, with its interaction energy calculated by the following equation:

$$U_i = \frac{q_i}{4\pi\epsilon_0\epsilon_r} \left[ \sum_k \frac{q_k}{r_{ik}} + \sum_j \left( \frac{Q_j}{r_{ij}} + \frac{\mu_j \mathbf{r}_{ij}}{r_{ij}^3} \right) \right] \quad (9)$$

where  $\epsilon_0$  is the permittivity of vacuum,  $q_i$  and  $q_k$  charges on the  $i$ th and  $k$ th ions (including phosphate on the DNA), respectively,  $r_{ik}$  the distance between them and  $\mathbf{r}_{ij}$  the displacement vector from the  $i$ th ion to the center of the  $j$ th cubic cell. The CPU time required is greatly reduced by the approximation scheme.  $\Delta\alpha$  thus calculated remains constant, as expected from the solution structure, which preserves ionic distributions in region I–III unchanged.

Figure 12 shows salt concentration  $c_s$  dependence of the anisotropy of the electric polarizability  $\Delta\alpha$  at a polymer concentration  $c_p = 0.60$  mM nucleotide residue plotted against the Debye length  $\kappa^{-1}$ .  $\Delta\alpha$  decreases monotonically with the addition of salt. The value  $\Delta\alpha = 6.5 \times 10^{-33}$  F m<sup>2</sup> at the highest salt concentration studied  $c_s = 4.8$  mM is comparable, for example, to the experimental  $\Delta\alpha$  of  $2.0 \times 10^{-33}$  F m<sup>2</sup> determined for a 64 base-pair DNA fragment at a concentration of 20  $\mu$ M nucleotide residue in a buffer system of 1 mM sodium cacodylate, 1 mM NaCl, and 0.2 mM EDTA at pH 7.1 by Diekmann et al.<sup>34</sup> despite some difference in the ionic environment. Data from other authors are shown in Table 2.

Stronger salt concentration dependence is observed in experiment, i.e., the induced dipole moment of DNA is inversely proportional to the square root of the ionic strength of the solution, tending to zero at infinite salt concentration.<sup>37–40</sup> The greatest reason for the discrepancy must be reduced internal fields in the conducting media.

#### 4.3. Effect of Electrophoretic Motion of Polyelectrolyte.

Let us estimate the effect of electrophoretic motion of a polyion

on the 33rd component of the polarizability tensor  $\alpha_{33} = \alpha_{zz}$  by calculating fluctuations of the  $z$  component of the dipole moment  $\mu_z$  generated around the center of the DNA cylinder:

$$\mu_z = \sum_{r=1}^{n^+} e(z_r^+ - Z) - \sum_{s=1}^{n^-} e(z_s^- - Z) \quad (10)$$

where  $z_r^+$ ,  $z_s^-$ , and  $Z$  are  $z$  coordinates of  $r$ th counterion,  $s$ th coion, and the center of the polyion cylinder, respectively, and  $n^+$  and  $n^-$  are numbers of counterions and coions, respectively. We assume that an initial configuration of ions has no dipole moment, i.e.,  $\mu_z = 0$  at  $t = 0$ . Fluctuations of  $\mu_z$  are then related to the displacements  $\Delta z_r^+$ ,  $\Delta z_s^-$ , and  $\Delta Z$  produced during time  $t$ . We also assume free diffusion for all the ion species. Let  $\alpha_{zz}^{\text{EP}}$  be the polarizability component calculated with electrophoretic motion of the polyion taken into consideration, then it is given by the following equation:

$$\begin{aligned} \alpha_{zz}^{\text{EP}} &= \langle (\mu_z)^2 \rangle / k_B T \\ &= \frac{1}{k_B T} \left\langle \left[ \sum_{r=1}^{n^+} e(\Delta z_r^+ - \Delta Z) - \sum_{s=1}^{n^-} e(\Delta z_s^- - \Delta Z) \right]^2 \right\rangle \\ &= \frac{e^2}{k_B T} \left\langle \left[ \sum_{r=1}^{n^+} \Delta z_r^+ - \sum_{s=1}^{n^-} \Delta z_s^- - (n^+ - n^-) \Delta Z \right]^2 \right\rangle \\ &= \frac{e^2}{k_B T} \left[ \sum_{r=1}^{n^+} \langle (\Delta z_r^+)^2 \rangle + \sum_{s=1}^{n^-} \langle (\Delta z_s^-)^2 \rangle + N^2 \langle (\Delta Z)^2 \rangle \right] \end{aligned} \quad (11)$$

where  $N = n^+ - n^-$  is the number of the phosphate charges on the DNA cylinder. The equation is further written as:

$$\begin{aligned} \alpha_{zz}^{\text{EP}} &= \frac{e^2}{k_B T} \left[ \sum_{r=1}^{n^+} 2d^+ t + \sum_{s=1}^{n^-} 2d^- t + N^2 2D_{||} t \right] \\ &= \frac{2e^2 t}{k_B T} [n^+ d^+ + n^- d^- + N^2 D_{||}] \end{aligned} \quad (12)$$

where  $d^+$  and  $d^-$  are counterion and coion diffusion constants, respectively, and  $D_{||} = D_{33}$ , the 33rd component of the diffusion tensor for the DNA cylinder. By putting  $D_{||} = 0$  on the right-hand of eq 12, we obtain the polarizability component calculated neglecting electrophoresis  $\alpha_{zz}^{\text{NEP}}$  as

$$\alpha_{zz}^{\text{NEP}} = \frac{2e^2 t}{k_B T} [n^+ d^+ + n^- d^-] \quad (13)$$

By taking the ratio of the equations, we obtain the following relation between  $\alpha_{zz}^{\text{EP}}$  and  $\alpha_{zz}^{\text{NEP}}$ :

**TABLE 2: Comparison with Experiment**

authors	$\Delta\alpha/10^{-33}$ F m <sup>2</sup>	DNA molecular weight <sup>a</sup> /base-pair	$c_p/\mu$ M nucleotide residue	$T/K$	ionic environment
this work	6.5	64	600	298	4.8 mM NaCl
Diekmann et al. <sup>b</sup>	2.0	64	~23	293	1 mM sodium cacodylate, 1 mM NaCl, 0.2mM EDTA
Stellwagen <sup>c</sup>	5.8 <sup>d</sup>	80	< 61	293	8 mM Tris, 0.8 mM EDTA
Elias and Eden <sup>e</sup>	4.0	64	~16	277	1.0 mM sodium phosphate

<sup>a</sup> Molecular weight used in experiment. <sup>b</sup> Reference 32. <sup>c</sup> Reference 34. <sup>d</sup> Corrected value for 64 base-pair assuming second power dependence on molecular weight. <sup>e</sup> Reference 36.

$$\alpha_{zz}^{\text{EP}} \approx \alpha_{zz}^{\text{NEP}} \left[ 1 + \frac{N^2 D_{\parallel}}{n^+ d^+ + n^- d^-} \right] \quad (14)$$

Equation 14 corresponds to the formulas derived by Fixman and Jagannathan<sup>41</sup> and Manning<sup>42</sup> for the primary convective effect.<sup>41</sup>

Electric conductivity is described in dielectric terms by an infinite dielectric constant  $\epsilon_r \rightarrow \infty$  and time or ensemble averages of eqs 12 and 13 diverge.<sup>43</sup> Out of  $n^+$  counterions and  $n^-$  coions, a greater number of ions exist in the bulk salt solution and contribute to the conductivity. It is the ions in the ion atmosphere that contribute to the permittivity or polarizability. We used the approximation of free diffusion of ions only to obtain eq 14 or to estimate the upper limit of the electrophoretic effect. The stronger an ion is bound to the polyion, the less it will be affected by the solvent flow.

By approximating  $d^+ = d^- = d$ , eq 14 becomes

$$\alpha_{zz}^{\text{EP}} \approx \alpha_{zz}^{\text{NEP}} \left[ 1 + \frac{N^2 D_{\parallel}}{(n^+ + n^-)d} \right] \quad (15)$$

In view of the strong interactions between condensed counterions and the polyion, if we consider them as a single entity, i.e.,  $N = 128 \times (1 - F_M) \approx 30$ , Figure 5 gives  $n^+ + n^- = 128 \times (2.5 - F_M) \approx 220$ . By using for  $d$  the diffusion constant of sodium ion in the infinitely dilute aqueous solution at 298 K, i.e.,  $D_{\text{Na}^+} = 1.3 \times 10^{-9} \text{ m}^2 \text{ s}^{-1}$  and for  $D_{\parallel}$ , that calculated from the formula<sup>44</sup>

$$D_{\parallel} = \frac{k_B T \ln(L/b)}{2\pi\eta_s L} \quad (16)$$

where  $\eta_s$  is the solvent viscosity and  $b$  the diameter of the DNA cylinder, i.e.,  $D_{\parallel} = 8.0 \times 10^{-11} \text{ m}^2 \text{ s}^{-1}$ , we obtain  $\alpha_{zz}^{\text{EP}} \approx 1.25 \alpha_{zz}^{\text{NEP}}$ . If we perform numerical simulation by taking hydrodynamic interactions between all the ion species into account,<sup>27</sup> we will be able to obtain more accurate estimates including the secondary convective effect.<sup>41</sup>

## 5. Conclusions

We have succeeded in the reproduction of the static electric polarizability of polyelectrolytes, not only in salt-free solution,<sup>19,20</sup> but also in salt solution by computer simulation. Introduction of partial polarizabilities enables us to clarify the origin of the induced dipole moment of polyelectrolytes.

In both salt-free and salt solutions, diffuse ion atmospheres play more important role in determining the dependence of the polarizability on salt or polymer concentration than condensed counterions. Contribution from the latter to the radial components of the polarizability tensor is very small, while that from the former is very large and cannot be neglected in the calculation of the anisotropy. In salt-free solutions, electric polarizability increases on dilution of polymer concentration as a result of the expansion of diffuse ion atmospheres. In salt

solutions, salt concentration dependence of the polarizability is ascribed to their contraction under pressure from the bulk salt solution.

## References and Notes

- (1) Kubo, R. *J. Phys. Soc. Jpn.* **1957**, *12*, 570.
- (2) Oosawa, F. *Biopolymers* **1970**, *9*, 677.
- (3) Oosawa, F. *Polyelectrolytes*; Marcel Dekker: New York, 1971.
- (4) Minakata, A.; Imai, N.; Oosawa, F. *Biopolymers* **1972**, *11*, 347.
- (5) Warashina, A.; Minakata, A. *J. Chem. Phys.* **1973**, *58*, 4743.
- (6) Minakata, A. *Ann. N.Y. Acad. Sci.* **1977**, *303*, 107.
- (7) Kikuchi, K.; Yoshida, M.; Maekawa, T.; Watanabe, H. *Chem. Phys. Lett.* **1991**, *185*, 335.
- (8) Kikuchi, K.; Yoshida, M.; Maekawa, T.; Watanabe, H. In *Colloid and Molecular Electrooptics 1991*; Jennings, B. R., Stoylov, S. P., Eds.; IOP Publishing: Bristol, 1992; pp 7–12.
- (9) Kikuchi, K.; Yoshida, M.; Maekawa, T.; Watanabe, H. *Chem. Phys. Lett.* **1992**, *196*, 57.
- (10) Yoshida, M.; Kikuchi, K. *J. Phys. Chem.* **1994**, *98*, 10303.
- (11) Yoshida, M.; Kikuchi, K. *Rep. Prog. Polym. Phys. Jpn.* **1996**, *39*, 115.
- (12) Washizu, H.; Kikuchi, K. *Chem. Lett.* **1997**, 651.
- (13) Washizu, H.; Kikuchi, K. *Rep. Prog. Polym. Phys. Jpn.* **1997**, *40*, 597.
- (14) Washizu, H.; Kikuchi, K. *Colloids Surf., A* **1999**, *148*, 107.
- (15) Kikuchi, K.; Washizu, H. In *Proceedings of Yamada Conference L: Polyelectrolytes*; Noda, I., Kokufuta, E., Eds.; Yamada Science Foundation: Osaka, 1999; pp 80–81.
- (16) Washizu, H.; Kikuchi, K. *Rep. Prog. Polym. Phys. Jpn.* **1999**, *42*, 367.
- (17) Washizu, H.; Kikuchi, K. *Chem. Phys. Lett.* **2000**, *320*, 277.
- (18) Washizu, H.; Kikuchi, K. *Rep. Prog. Polym. Phys. Jpn.* **2000**, *43*, 615.
- (19) Kikuchi, K. In *Physical Chemistry of Polyelectrolytes*; Radeva, Ts., Ed.; Marcel Dekker: New York, 2001; pp 223–243.
- (20) Washizu, H.; Kikuchi, K. *J. Phys. Chem. B* **2002**, *106*, 11329.
- (21) Kellogg, O. D. *Foundations of Potential Theory*; Dover: New York, 1954; Chapter 3.
- (22) Oosawa, F. *J. Polym. Sci.* **1957**, *23*, 421.
- (23) Manning, G. S. *J. Chem. Phys.* **1969**, *51*, 924.
- (24) Ramanathan, G. V.; Woodbury, C. P., Jr. *J. Chem. Phys.* **1982**, *77*, 4133.
- (25) Washizu, H.; Kikuchi, K. In *Molecular and Colloidal Electrooptics*; Stoimenova, M., Ed.; CRC Press: Boca Raton, to be published in 2006.
- (26) Grycuk, T.; Antosiewicz, J.; Porschke, D. *J. Phys. Chem.* **1994**, *98*, 10881.
- (27) Antosiewicz, J.; Porschke, D. *J. Phys. Chem. B* **1997**, *101*, 4478.
- (28) Arnott, S.; Hukins, D. W. L. *Biochem. Biophys. Res. Commun.* **1972**, *47*, 1504.
- (29) Manning, G. S. *Physica A* **1997**, *247*, 196.
- (30) Odijk, T. *Physica A* **1991**, *176*, 201.
- (31) Manning, G. S. *Physica A* **1996**, *231*, 236.
- (32) Manning, G. S. *Biophys. Chem.* **1978**, *9*, 65.
- (33) Saito, M. *Mol. Simul.* **1992**, *8*, 321.
- (34) Diekmann, S.; Hillen, W.; Jung, M.; Wells, R. D.; Porschke, D. *Biophys. Chem.* **1982**, *15*, 157.
- (35) Stellwagen, N. *Biopolymers* **1981**, *20*, 399.
- (36) Elias, J. G.; Eden, D. *Macromolecules* **1981**, *14*, 410.
- (37) Hogan, M.; Dattagupta, N.; Crothers, D. M. *Proc. Natl. Acad. Sci. U.S.A.* **1978**, *75*, 195.
- (38) Hornick, C.; Weill, G. *Biopolymers* **1971**, *10*, 2345.
- (39) Yamaoka, K.; Matsuda, K.; Takarada, K. *Bull. Chem. Soc. Jpn.* **1983**, *56*, 927.
- (40) Rau, D. C.; Charney, E. *Biophys. Chem.* **1983**, *17*, 35.
- (41) Fixman, M.; Jagannathan, S. *J. Chem. Phys.* **1981**, *75*, 4048.
- (42) Manning, G. S. *J. Chem. Phys.* **1989**, *90*, 5704.
- (43) Landau, L. D.; Lifshitz, E. M. *Electrodynamics of Continuous Media*; Pergamon Press: London, 1960.
- (44) Doi, M.; Edwards, S. F. *The Theory of Polymer Dynamics*; Clarendon Press: Oxford, 1986.